Influence of surface electronic structure on quantum friction between Ag(111) slabs

Despoja, Vito; Silkin, Vyacheslav M.; Echenique, Pedro M.; Šunjić, Marijan

Journal article, Published version
Rad u časopisu, Objavljena verzija rada (izdavačev PDF)

Repository / Repozitorij:

Repository of the Faculty of Science - University of Zagreb

Influence of surface electronic structure on quantum friction between Ag(111) slabs

Vito Despoja,[1,2,3] Vyacheslav M. Silkin,[1,3,4] Pedro M. Echenique,[1,3] and Marijan Šunjić[1,2]

[1]*Donostia International Physics Center (DIPC), P. Manuel de Lardizabal, 4, 20018 San Sebastián, Spain*

[2]*Department of Physics, University of Zagreb, Bijenička 32, HR-10000 Zagreb, Croatia*

[3]*Departamento de Fisica de Materiales and Centro Mixto CSIC-UPV/EHU, Facultad de Ciencias Químicas,*
Universidad del Pais Vasco UPV/EHU, Apto. 1072, 20080 San Sebastián, Spain

[4]*IKERBASQUE, Basque Foundation for Science, 48011 Bilbao, Spain*

The theoretical formulation developed in Phys. Rev. B **83**, 205424 (2011) is applied to explore how surface electronic structure modifies the noncontact friction force between two silver slabs. We find that the friction shows three distinct regimes for different thicknesses. For very thin slabs $N = 1$–7 monolayers (ML) quantum friction vs velocity shows oscillations which are due to the quantum size effect. At about $10ML$ friction rapidly increases because the surface state energies fall below E_F, which opens a new intraband electron-hole excitation channel. And for $N > 15$ the friction is strongly enhanced due to the excitation of acoustic surface plasmons.

I. INTRODUCTION

A charged or neutral object moving close to a dielectric surface, e.g., parallel to a metallic slab, can excite electronic (or other phonon) modes at the surface. This can cause it to lose kinetic energy and slow down if no external driving force acts on the object. This and related phenomena, known as energy loss or stopping power, were extensively studied by many authors [1–6]. Moreover, in the last decade much attention has been paid to a similar dissipative phenomenon, the so-called quantum or van der Waals friction, i.e., frictional forces between two dielectrics without direct contact, moving with parallel velocity, at zero or finite temperature. This is not only an intriguing theoretical problem but also a potentially relevant phenomenon, e.g., affecting the behavior of micromechanical devices (MEMS) [7–13] of nanometer dimensions. In this situation an obvious question can be posed: Is this process physically feasible, since translation symmetry is not broken and dielectrics are not in contact, and if it is, which mechanism is responsible for friction? A number of authors approached this question [14–19] with different and often contradictory conclusions, even questioning the possibility of quantum friction [20] as formulated by Pendry [16], in spite of several extensive studies, e.g., by Persson and Volokitin [17,18,21–23]. Another group of researchers investigated the impact of a fluctuating electromagnetic field on attractive conservative forces and heating rate, responsible for the dissipative force, between a thick plate or a particle moving parallel to the dielectric surface [24]. This research also resulted in some disagreement with the previously cited work. Another study of Casimir friction forces between dielectric plates moving parallel to each other [25] provided formally the same expressions as in the previous investigations.

In order to elucidate these intriguing questions, in a previous paper [26] we have proposed an alternative formulation of quantum friction (in the $T = 0$ and nonretarded limit) based on the diagramatic perturbation expansion. The idea was to evaluate the coupling between Doppler-shifted charge density fluctuations in the slabs in relative parallel motion, which are described by nonlocal surface response functions, derived, e.g., within the random-phase approximation (RPA). The

resulting expressions look formally the same as those in Refs. [16–18,21–23] obtained using matching procedures, but now surface response functions $R_i(Q,\omega)$ are derived from nonlocal response functions of the slabs $R_i(Q,\omega,z,z')$. This enables us to take into account the details of the surface electronic structure, including realistic surface density profiles, and excitations in the slabs.

The main objective of this paper is to apply formulation developed in Ref. [26] to investigate how microscopic electronic structure, such as a series of intraband excitation channels which are the consequence of quantum size effects or acoustic surface plasmons (APS) (which are a consequence of the existence of surface states) influence noncontact friction force between two silver slabs in relative motion. We showed that in some limit semilocal or even fully nonlocal (RPA) descriptions of the surface response in a jellium model are not sufficient to describe quantum friction. For example, in noble metal surfaces the main contribution to quantum friction comes from excitation of ASP. So even if $R_i(Q,\omega)$ are calculated fully nonlocally if the model does not include ASP, the friction force will be strongly underestimated. In Ref. [27] the influence of surface electronic structure on the Casimir force between silver slabs was investigated. It was shown that the changes from the jellium to the Chulkov model enhance Casimir energy, but the effects is much less visible than in the case of the friction force.

In this paper we find that the friction force vs relative velocity for ultrathin films, up to $10ML$ thicknesses, shows oscillations with the maxima that can be related to the Fermi velocities in the quantum well states, for thicker slabs at some point the intraband transitions within the surface states suddenly enhance the friction force, and finally for thick slabs or semi-infinite metals the main contribution to friction force comes from the excitation of acoustic surface plasmons. We conclude that the details of the electronic excitation spectra and intensities, calculated for slabs of different thicknesses in the jellium [28] and Chulkov [29] models, are crucial for the correct interpretation of different features appearing in the friction force.

In Sec. II we briefly present the derivation of the energy dissipation rate and friction force, based on the nonlocal dynamical response functions of the slabs [26]. We describe

the system consisting of two sliver slabs of the same thickness, separated by the distance d. The wave functions and response functions calculation are briefly discussed.

In Sec. III we present the electronic band structure and electronic excitation spectra calculated in the two models: jellium, with the density corresponding to bulk silver, and the Chulkov model, which includes lattice structure in the perpendicular direction. The electronic excitation intensities are shown, in both models, for slabs with different thicknesses modelled on the results of Refs. [28–30]. We apply these results to evaluate and discuss dissipation and friction between two silver slabs moving with parallel relative velocity. We observe three different regimes for the friction force with the increasing slab thicknesses: quantum size effect regime, quantum friction anomaly, and the acoustic surface plasmon regime. We explain this interesting behavior by referring to the changes in the electronic structure of the slabs with varying thicknesses.

In Sec. IV we present the conclusions.

II. THEORETICAL FORMULATION

Quantum friction between two nonoverlapping metallic or dielectric slabs has been extensively studied by using various approaches, in the retarded and nonretarded limits, and for zero and finite temperature [16–18,21–23]. Also the surface electronic response was treated locally but also by using approximate response functions which include nonlocal corrections, e.g., electron-hole pair excitations [31,32]. An alternative formulation developed in Ref. [26] is restricted to $T = 0$ and the nonretarded limit; however, it is expressed in terms of surface response and correlation functions which reflect the quantum mechanical nature of friction force more directly. Moreover, this formulation is easily adapted to different levels of accuracy; e.g., surface response function can be calculated in local approximation, but it can also be calculated by using *ab initio* methods which include realistic surface orbital and band structure [33]. Here we will briefly present some crucial steps in this alternative formulation of quantum friction.

The formulation is restricted to zero temperture ($T = 0$) and nonretarded ($c \to \infty$) limits. $T = 0$ limit is justified because here we analyze how the electronic excitations contribute to quantum friction. Electronic excitations responsible for phenomena described below (intraband electron-hole excitations) are in the 10-100 meV energy range and contribute to friction for the relative velocities $v \lesssim v_F$, where the v_F is the characteristic Fermi velocity, e.g., in the noble metals considered here. Such electronic modes are still rigid, e.g., at room temperature, and thermal fluctuations can be neglected. However, optical or acoustic phonons which contribute to the quantum friction at much lower velocities $v \ll v_F$ can be multiply populated at room temperature and their inclusion causes that quantum friction becomes temperature dependent. Nonretarded limit is justified for small separations between the slabs ($d \approx \frac{1}{Q}$) when the evanescent modes ($\omega < Qc$) dominantly contribute to the friction force. However, for large separations ($d \gg \frac{1}{Q}$) only the radiative modes ($\omega > Qc$) contribute to quantum friction and the nonretarded limit becomes inadequate. Here we shall restrict ourselves to small
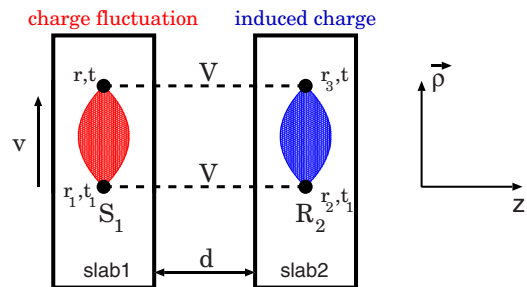

FIG. 1. (Color online) Process in which charge density fluctuation is created in the slab 1 and induces a potential in slab 2.

separations ($d = 1.5$ nm) when the effects of retardation can be safely neglected.

The geometry of the system is schematically shown in Fig. 1, where slabs 1 and 2 represent metallic slabs with nonoverlapping electronic densities and d is the distance between their jellium edges. Suppose that the slab 1 is moving parallel to slab 2 with relative velocity $\mathbf{v}$ and that a charge density fluctuation is spontaneously created in slab 1 at the moment t_1, as sketched in Fig. 1.

Propagating in time between t_1 and t it induces charge density fluctuations in the right slab with which it can subsequently interact. In such a process slab 1 can be considered as the source which is transferring energy to slab 2, and in analogy with Eqs. (3) and (4) of Ref. [26], the energy loss rate operator in this process can be written as

$$\hat{P}_{12} = \int d\mathbf{r} \int d\mathbf{r}_1 \int_{-\infty}^{\infty} dt_1 \, \hat{\rho}(\mathbf{r},t) V(\mathbf{r},\mathbf{r}_3)$$
$$\times \frac{d}{dt} R_2(\mathbf{r}_3,\mathbf{r}_2,t,t_1) V(\mathbf{r}_2,\mathbf{r}_1) \hat{\rho}(\mathbf{r}_1,t_1), \quad (1)$$

where R_2 is the retarded response function of the right slab and $\hat{\rho}(\mathbf{r},t)$ and $\hat{\rho}(\mathbf{r},t)$ are density operators which represent quantum mechanical charge density fluctuations created and annihilated at points $(\mathbf{r}_1,t_1)$ and $(\mathbf{r},t)$, respectively. Energy transfer rate from slabs 1 to 2 can be obtained by taking the ground-state matrix element of Eq. (1):

$$P_{12} = \langle \hat{P}_{12}(t) \rangle = \int d\mathbf{r} \int d\mathbf{r}_1 \int_{-\infty}^{\infty} dt_1 S_1(\mathbf{r},\mathbf{r}_1,t,t_1) V(\mathbf{r},\mathbf{r}_3)$$
$$\times \frac{d}{dt} R_2(\mathbf{r}_3,\mathbf{r}_2,t,t_1) V(\mathbf{r}_2,\mathbf{r}_1), \quad (2)$$

where

$$S_1(\mathbf{r},\mathbf{r}_1,t,t_1) = \langle \hat{\rho}(\mathbf{r},t)\hat{\rho}(\mathbf{r}_1,t_1) \rangle + \langle \hat{\rho}(\mathbf{r}_1,t_1)\hat{\rho}(\mathbf{r},t) \rangle \quad (3)$$

is the correlation function of slab 1 which represents real charge density fluctuations. We note that in the inertial system of the right slab, the charge density in slab 1, apart from the fluctuations, has an additional parallel component of motion, so all parallel coordinates in slab 1 have to be transformed as

$$\boldsymbol{\rho} - \boldsymbol{\rho}_1 \to \boldsymbol{\rho} - \boldsymbol{\rho}_1 - \mathbf{v}(t - t_1). \quad (4)$$

Explicitly, the correlation function (3) then becomes

$$S_1(\mathbf{r},\mathbf{r}_1,t,t_1) = S_1(z,z_1,\boldsymbol{\rho} - \mathbf{v}t,\boldsymbol{\rho}_1 - \mathbf{v}t_1,t,t_1). \quad (5)$$

After inserting Eq. (5) into Eq. (2) and the Fourier transformation in parallel coordinates $\boldsymbol{\rho}$ and in time t we get the formula

for energy transfer rate per unit area from slab 1 to slab 2:

$$P_{12} = -i\hbar \int_{-\infty}^{\infty} dz \int_{-\infty}^{\infty} dz_1 \int \frac{d\mathbf{Q}}{(2\pi)^2} \int_{-\infty}^{\infty} \frac{d\omega}{2\pi}$$

$$\times \omega' S_1(\mathbf{Q},|\omega|,z,z_1) V(\mathbf{Q},z,z_3)$$

$$\times R_2(\mathbf{Q},\omega',z_3,z_2) V(\mathbf{Q},z_2,z_1). \quad (6)$$

After using the definitions

$$V(\mathbf{Q},z,z_3) = v_Q e^{-Q(z_3-z)},$$

$$V(\mathbf{Q},z_2,z_1) = v_Q e^{-Q(z_2-z_1)}. \quad (7)$$

where $v_Q = \frac{2\pi e^2}{Q}$, the definition of the surface correlation function

$$S_1(\mathbf{Q},|\omega|) = v_Q \int dz dz_1 e^{Qz} S_1(\mathbf{Q},|\omega|,z,z_1) e^{Qz_1}, \quad (8)$$

and the surface response function [34]

$$R_2(\mathbf{Q},\omega) = v_Q \int dz_2 dz_3 e^{-Qz_2} R_2(\mathbf{Q},\omega,z_2,z_3) e^{-Qz_3}, \quad (9)$$

Eq. (6) can be written as

$$P_{12} = -i\hbar \int \frac{d\mathbf{Q}}{(2\pi)^2} \int_{-\infty}^{\infty} \frac{d\omega}{2\pi} e^{-2QD} S_1(\mathbf{Q},|\omega|)$$

$$\times \omega' R_2(\mathbf{Q},\omega'). \quad (10)$$

Using the connection between the surface correlation function S and the imaginary part of the surface response function R

$$S_1(\mathbf{Q},|\omega|) = \text{sgn}\omega \text{Im} R_1(\mathbf{Q},\omega) \quad (11)$$

Eq. (10) can be written as

$$P_{12} = -i\hbar \int \frac{d\mathbf{Q}}{(2\pi)^2} \int_{-\infty}^{\infty} \frac{d\omega}{2\pi} e^{-2Qd} \omega' \text{sgn}\omega$$

$$\times \text{Im} R_1(\mathbf{Q},\omega) R_2(\mathbf{Q},\omega'). \quad (12)$$

Finally, as the imaginary part of surface excitation propagator (22) is an odd function of frequency, P_{12} given by Eq. (12) is a real quantity

$$P_{12} = \hbar \int \frac{d\mathbf{Q}}{(2\pi)^2} e^{-2Qd} \int_{-\infty}^{\infty} \frac{d\omega}{2\pi} \omega' \text{sgn}\omega$$

$$\times \text{Im} R_1(\mathbf{Q},\omega) \text{Im} R_2(\mathbf{Q},\omega'). \quad (13)$$

We see that if the charge fluctuation is created in slab 1 with the energy ω it can create excitations in slab 2 with the energy $\omega' = \omega + \mathbf{vQ}$. This is expected, namely, ω is the energy in the inertial system of slab 1, but in the inertial system of the right slab it is Doppler shifted by $\mathbf{vQ}$.

In Eq. (13) we have calculated the energy transferred from slab 1 to slab 2. However, part of this energy belongs to the quantum mechanical (or thermal, at $T \neq 0$) fluctuations, the energy which fluctuates between the slabs. So a certain amount of energy transferred to slab 2 will be reversibly returned back to slab 1. We can calculate this energy by going into the inertial system of slab 1 and forget for the moment slab 2. Sitting in the inertial system of slab 1 we know that it is in the quantum mechanical (and thermodynamical) equilibrium with the environment (in this case with the slab 2). So, the energy just fluctuates between the slab 1 and the environment; i.e., all energy given to the environment (slab 2) will be reversibly

returned to slab 1. The energy given to the environment (slab 2) can be calculated using exactly the same ideas as before, except that now the slab 2 is moving with the velocity $-\mathbf{v}$ and the slab 1 is at rest. Therefore, following the same procedure (1–13) with the response functions of the slab 2 transformed as

$$R_2(\mathbf{r},\mathbf{r}_1,t,t_1) = R_2(z,z_1,\boldsymbol{\rho}+\mathbf{v}t,\boldsymbol{\rho}_1+\mathbf{v}t_1,t,t_1) \quad (14)$$

gives the energy that is reversibly given to the slab 2:

$$P'_{12} = \hbar \int \frac{d\mathbf{Q}}{(2\pi)^2} e^{-2Qd} \int_{-\infty}^{\infty} \frac{d\omega}{2\pi} \omega \, \text{sgn}\omega$$

$$\times \text{Im} R_1(\mathbf{Q},\omega) \text{Im} R_2(\mathbf{Q},\omega'). \quad (15)$$

This means that the energy which is irreversibly given to the slab 2 or dissipated energy can be obtained by subtracting the reversible contribution P'_{12} from the total energy transfer P_{12}:

$$P_1^{\text{diss}} = P_{12} - P'_{12} = \hbar\mathbf{v} \int \frac{d\mathbf{Q}}{(2\pi)^2} \mathbf{Q} \, e^{-2Qd}$$

$$\times \int_{-\infty}^{\infty} \frac{d\omega}{2\pi} \text{sgn}\omega \, \text{Im} R_1(\mathbf{Q},\omega) \text{Im} R_2(\mathbf{Q},\omega'). \quad (16)$$

Expression (16) represents the dissipated energy if the charge fluctuation is spontaneously created in the slab 1. However, the charge fluctuation can also be spontaneously created in the slab 2, and then the corresponding dissipated energy can be obtained from Eq. (16) with $1 \leftrightarrow 2$ and $\mathbf{v} \leftrightarrow -\mathbf{v}$. Therefore the total dissipated energy can be written as

$$P_{\text{diss}} = P_1^{\text{diss}} + P_2^{\text{diss}} = \hbar\mathbf{v} \int \frac{d\mathbf{Q}}{(2\pi)^2} \mathbf{Q} e^{-2Qd}$$

$$\times \int_{-\infty}^{\infty} \frac{d\omega}{2\pi} \, \text{sgn}(\omega) [\text{Im} R_1(\mathbf{Q},\omega) \text{Im} R_2(\mathbf{Q},\omega')$$

$$+ \text{Im} R_1(\mathbf{Q},\omega') \text{Im} R_2(\mathbf{Q},\omega)]. \quad (17)$$

Changing the arguments $\omega + \mathbf{vQ} \rightarrow \omega$ and $\mathbf{Q} \rightarrow -\mathbf{Q}$ in the second term of Eq. (20) the frequency integration becomes

$$\hbar\mathbf{vQ} \int_{-\infty}^{\infty} \frac{d\omega}{2\pi} [\text{sgn}(\omega) - \text{sgn}(\omega + \mathbf{vQ})]$$

$$\times \text{Im} R_1(\mathbf{Q},\omega) \text{Im} R_2(\mathbf{Q},\omega + \mathbf{vQ})$$

$$= 2\hbar\mathbf{vQ} \int_0^{\mathbf{Qv}} \frac{d\omega}{2\pi} \text{Im} R_1(\mathbf{Q},\omega) \text{Im} R_2(\mathbf{Q},\mathbf{vQ}-\omega), \quad (18)$$

which leads to a more compact expression for the dissipated energy,

$$P_{\text{diss}} = 2\hbar\mathbf{v} \int \frac{d\mathbf{Q}}{(2\pi)^2} e^{-2Qd} \mathbf{Q} \int_0^{\mathbf{Qv}} \frac{d\omega}{2\pi}$$

$$\times \text{Im} R_1(\mathbf{Q},\omega) \text{Im} R_2(\mathbf{Q},\mathbf{vQ}-\omega). \quad (19)$$

After inclusion of the higher order terms (multiple processes where the charge density fluctuations in slabs 1 and 2 successively induce each other several times before the energy is being dissipated, as described in detail in Ref. [26]) the dissipated energy can be written as

$$P_{\text{diss}} = 2\hbar\mathbf{v} \int \frac{d\mathbf{Q}}{(2\pi)^2} \mathbf{Q} e^{-2Qd} \int_0^{\mathbf{Qv}} \frac{d\omega}{2\pi} \times$$

$$\times \frac{\text{Im} R_1(\mathbf{Q},\omega) \, \text{Im} R_2(\mathbf{Q},\mathbf{vQ}-\omega)}{|1 - e^{-2Qd} \text{Im} R_1(\mathbf{Q},\omega) \, \text{Im} R_2(\mathbf{Q},\mathbf{vQ}-\omega)|^2}. \quad (20)$$

This expression formally agrees with the quantum friction formulas developed in Refs. [16–20,22,23] except that in these formulas instead of surface excitation propagators R_i enter reflectivity amplitudes (reflection coefficients) R_s^i and R_p^i for s and p polarized electromagnetic fields. However, considering that in the nonretarded limit ($c \to \infty$) the reflection coefficient $R_s^i = 0$, and R_p^i becomes equal to surface response functions R_i, as briefly derived in Sec. IV of Ref. [35], this expression becomes exactly equal to quantum friction formulas presented in other publications.

In our case, for larger slab separations d we shall be able to neglect these higher order contributions, since, e.g., in the n-th order, they decrease as $(e^{-2Qd})^n$. If we use the expression which relates the friction force and dissipated power $P = -\mathbf{F}\mathbf{v}$, and suppose that $\mathbf{v} = v\mathbf{x}$, the friction force formula becomes

$$F_x = \frac{\hbar}{\pi^3} \int_0^\infty Q_x dQ_x \int_{-\infty}^\infty dQ_y \, e^{-2Qd} \int_0^{vQ_x} d\omega$$
$$\times \mathrm{Im}[R_1(\mathbf{Q},\omega)] \, \mathrm{Im}[R_2(\mathbf{Q}, vQ_x - \omega)]. \quad (21)$$

If we use the connection between the surface spectral function and the imaginary part of the surface response function (22), which is for $\omega > 0$ given by

$$S_i(\mathbf{Q},\omega) = \mathrm{Im}[R_i(\mathbf{Q},\omega)]; \; i = 1,2, \quad (22)$$

the functions in the numerator of Eq. (21) can be replaced by the surface spectral functions S_i; $i = 1,2$.

In the following we shall consider two silver slabs with the density defined by the bulk silver Fermi velocity $v_F = 1.4 \times 10^6$ m/s, separated by the distance $d = 5$ nm. The slab thicknesses are given by the number N of monolayers, with $1 \leqslant N \leqslant 10$ and $N = 17$, with each monolayer thickness corresponding to 4.434 a.u., which is the bulk silver (111) atomic plane separation. We shall closely follow the methods of Ref. [30] and obtain similar results.

The surface response functions $R_i(Q,\omega)$; $i = 1,2$ contain the intensities of all (collective and single-particle) electronic excitations in the metallic surfaces. Calculation of the functions $R_i(Q,\omega)$ is described in detail in Refs. [28,36,37], and here we shall only describe it briefly. First we suppose that the metal slabs are translationally invariant in the direction parallel to the surface, i.e., that the electron wave functions in that direction are plane waves with energies $\frac{\hbar^2 \mathbf{K}^2}{2m}$, and $\mathbf{K} = \{K_x, K_y\}$ is a two-dimensional (2D) wave vector. In the z direction where the symmetry is broken, the wave functions are calculated by using two different models. In the first model the system is described by Kohn-Sham wave functions $\phi_n(z)$ and energy levels E_n which are self-consistent solutions of the one-dimensional Kohn-Sham equation for the *jellium* slabs of various thicknesses. The positive background density is defined by Wigner-Seitz radius r_s [38]. For the exchange and correlation potential we use the Local Density Approximation (LDA) Wigner formula. In the second model the wave functions $\phi_n(z)$ and energy levels E_n are solutions of the Chulkov model potential, as described in Ref. [29]. From Kohn-Sham or Chulkov wave functions $\phi_n(z)$ and energy levels E_n we calculate the Fourier transforms of noninteracting electron response functions $\chi_i^0(Q,\omega,z,z')$; $i = 1,2$. Therefore, intraband $n = m$ contributions to χ_i^0's are

similar to quasi-2D Lindhard functions, but we also include the interband $n \neq m$ contributions. Screened response functions $\chi_i(Q,\omega,z,z')$; $i = 1,2$ are calculated from χ_i^0's by solving matrix equations $\chi_i = \chi_i^0 + \chi_i^0 V \chi_i$, where, at the RPA level of approximation, V is the 2D Fourier transform of bare Coulomb interaction $V(Q) = \frac{2\pi}{Q} e^{-Q|z-z'|}$. Surface response functions $R_i(Q,\omega)$ represent induced dynamically screened Coulomb interaction at the metallic surface, which can be obtained from the screened response functions $\chi_i(Q,\omega,z,z')$ as

$$R_i(Q,\omega) = \frac{1}{v_Q} W_i^{ind}(Q,\omega,z=0,z'=0)$$

$$= v_Q \int_{-L_i}^0 dz_1 dz_2 \, e^{Q(z_1+z_2)} \chi_i(Q,\omega,z_1,z_2);$$

$$i = 1,2.$$

From Eq. (21) it is obvious that the contributions to the friction force come from the overlap integral between two Doppler-shifted spectral functions $S_1(\mathbf{Q},\omega)$ and $S_2(\mathbf{Q}, Q_x v - \omega)$. As the velocity v increases the overlap integral and the friction force increase. However, the metallic slab surface spectral functions contain a variety of different features, such as intra- or interband electron hole transitions, surface and/or acoustic plasmons, etc., which then lead to some interesting features in the friction force, as discussed in detail in Sec. III.

III. RESULTS AND DISCUSSION

In order to have better insight on how the metallic electron structure influences the friction forces we shall first briefly present some important details of the electronic band structure and excitation spectra. Figure 2 shows quantized electronic bands for $N = 7$ with jellium results on the left and Chulkov model results on the right side. In the latter case we observe the appearance of two (even-odd) quantum-well states (shown
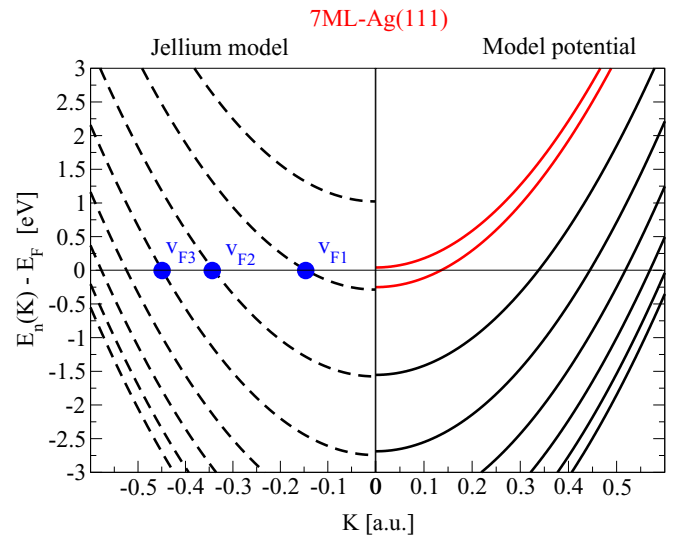
FIG. 2. (Color online) Quantized electronic bands in a $7ML$-thick silver slab. Left (right) side presents bands obtained in the jellium (Chulkov) model. Red (gray) lines highlight the even and odd energy bands evolving, upon the slab thickness increase, into a partially occupied s-p surface state of the semi-infinite Ag(111) crystal.
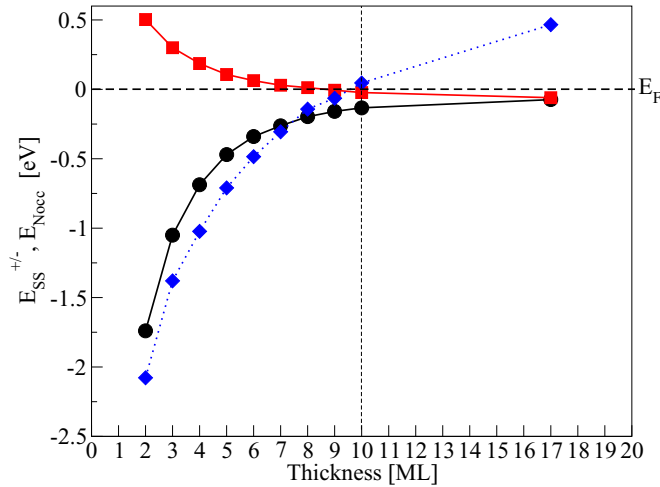
FIG. 3. (Color online) Energies at $K = 0$ of even surface state (black dots) and odd surface state (red [gray] squares) in the Chulkov model and topmost occupied state in the jellium model (blue [gray] diamonds) as functions of metallic slab thickness.

by the red [gray] lines) evolving into the s-p surface state upon increase of the slab thickness.

Figure 3 presents the energies of even (black dots) and odd surface states (red [gray] squares) as functions of metallic slab thickness. We can notice how the energy difference between even and odd surface states decreases as the slab thickness increases. We can also notice how the odd surface state, approaching the Fermi level E_F and for $N = 9$–10, becomes partially occupied. At the same time energy of the highest occupied state in the jellium model, shown by blue (gray) diamonds, becomes unoccupied. We shall see that this effect will be responsible for an unusual behavior of quantum friction at $N = 10$, when friction force in the jellium model drops down and in the Chulkov model becomes enhanced.

Calculated electron wave functions in these two models can be used to obtain excitation spectra of individual slabs. The overlap between these spectra, as formulated in Eq. (21), then gives the friction force. As an example, the right-hand graph in Fig. 4(a) shows the low-energy spectra of a $8ML$-thick silver slab in the jellium model, and the left-hand graph shows its mirror image. In the right-hand graph we see a series of peaks corresponding to intraband electron-hole transitions within discrete bands shown in Fig. 2. As the velocity increases, the left-hand graphs translate to the right, as shown in Figs. 4(b), 4(c), and 4(d), and the peaks start to overlap. This leads to the oscillatory behavior in the friction force, as will be discussed in detail in Sec. III A. The origin of this oscillatory behavior in the friction force can also be easily understood by analyzing the intensities of the low-lying electronic excitations in metallic slabs, reported in Fig. 5. Equation (21) shows that only the overlap integral of the two spectra contributes to the friction force. In terms of the spectra shown in Fig. 5, this means that each spectrum should be first reflected about the momentum axis and then, as the velocity increases, rotated in a clockwise direction. Only the cross section between the original and reflected-rotated spectra contributes to the friction force. By observing the spectral intensities we notice the bright linearly dispersive features
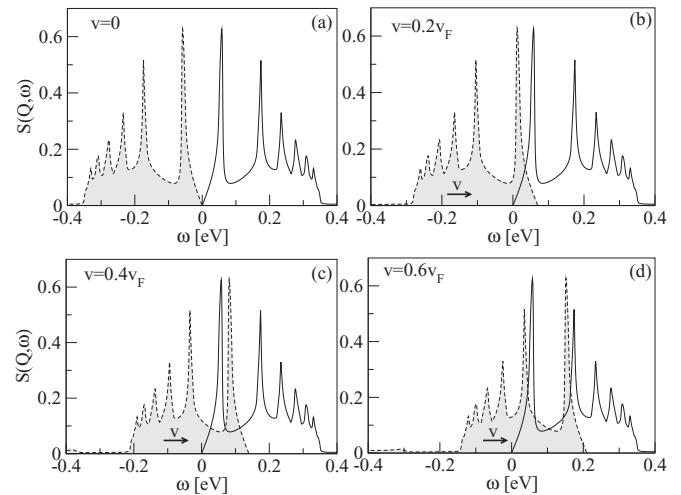

FIG. 4. Spectral function overlap for different relative velocities; (a) $v = 0$, (b) $v = 0.2v_F$, (c) $v = 0.4v_F$, and (d) $v = 0.6v_F$. Film thicknesses, in silver atomic monolayer units, are $L_1 = L_2 = 8ML$, which corresponds to 1.5 nm. Parallel wave vector is $Q = 0.02$ a.u. Series of peaks correspond to intraband electron-hole transitions within discrete bands.

which correspond to intraband electron-hole transitions within discrete bands (which give rise to the peaks in Fig. 4). Exactly for the velocity v at which these bright lines overlap, the friction force shows a maximum.

In Figs. 6(a) and 6(b) we show electronic excitation intensities for different slab thicknesses (7,8 and $9ML$) in both jellium and Chulkov models, respectively. Similar spectral intensities were also presented in Ref. [30]. Jellium spectra show series of linearly dispersive bright features which correspond to intraband electron-hole transitions within discrete bands shown in Fig. 2. However, in the Chulkov model we can also notice almost horizontally dispersing bright features which correspond to interband electron-hole transitions between surface states. It is important to notice how the lowest intraband branch disappears for the $10ML$-thick jellium slab. Exactly this effect will be responsible for a rapid friction force reduction at this thickness, as will be described in detail in Sec. III B.

A. Quantum size effect

In this section we shall use the previous conclusions to analyze how the friction force between two metallic layers of different thicknesses depends on their relative velocity. We shall first consider slabs with thicknesses between $4ML$ and $9ML$. The resulting friction forces are shown in Fig. 7. We shall show that the observed oscillations can be interpreted assuming that the friction arises from electron-hole excitations within the quantized levels in Fig. 2.

In Fig. 7 we see that the force between $4ML$-thick slabs shows a maximum slightly below v_F. For thicker slabs this maximum shifts to lower velocities, for $6ML$ a new maximum appears which also shifts down as the velocity increases, and for 7, 8, and $9ML$ there are three well-defined maxima.

The origin of these maxima can be easily understood by analyzing the intensities of the low-lying electronic excitations in metallic slabs, shown in Fig. 5. As already mentioned,
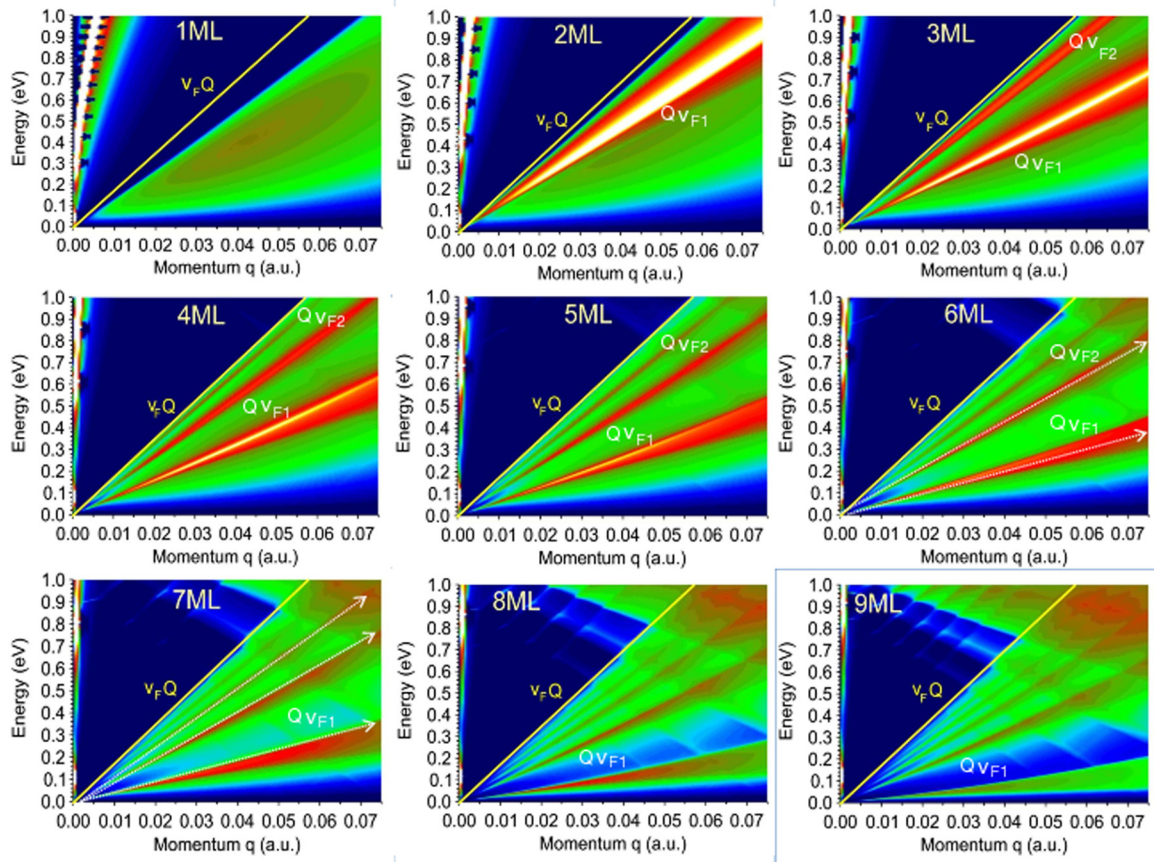
FIG. 5. (Color online) Intensities of the low-lying electronic excitations in silver slabs of different thicknesses, in the jellium model. The color intensity is in arbitrary units and scales linearly as 0, black; 0.2, light blue; 0.4, light green; 0.6, red; 0.8, yellow; and 1.0, white.

the transitions where spectral functions in Eq. (21) overlap contribute mainly to the friction force. This was illustrated in Fig. 4 which shows the overlaps between the spectra of single-particle excitations calculated in the jellium model as functions of the relative velocity v. Sharp peaks in Fig. 4 correspond to bright linearly dispersive features in Fig. 5 which represent intraband electron-hole transitions within discrete bands. Assuming that they originate from the level with the Fermi velocity v_{Fn}, shown by blue (gray) dots in Fig. 2, the dispersion relations of such single-particle transitions can be approximated as

$$\omega_n(Q) = v_{Fn}Q \,, \tag{23}$$

where the Fermi velocity in the discrete band n is

$$v_{Fn} = \sqrt{\frac{2}{m_n^*}(E_F - E_n)} \tag{24}$$

and E_n is the bottom ($\mathbf{K} = 0$ value) of the $n$rmth band. Therefore, it is obvious from Eq. (21) that the friction force will show a peak when the overlap between the two spectra is maximum, and this is when the relative velocities satisfy the resonant condition

$$v_{res} = v_{Fn} + v_{Fm}; \; n,m = 1,2,\ldots. \tag{25}$$

Now we can check how the resonant condition (25) applies to the results in Fig. 7. As can be noticed in Fig. 5, for $4ML$-thick silver slabs the Fermi velocity v_{F1} is about half the bulk

Fermi velocity v_F, so according to Eq. (25) the friction force shows a maximum near the Fermi velocity $v_F = 2v_{F1}$, as we indeed see in Fig. 7. As the film thickness increases the Fermi velocity v_{F1} decreases, so the first maximum at $2v_{F1}$ should also shift to lower values. Indeed, in Fig. 7 we can follow how the position of the first maximum for $5,6,7,\ldots,ML$ slabs decreases. For the $6ML$ slab we can notice the appearance of a second maximum which corresponds to the resonant condition $v_{F1} + v_{F2}$, and for $7ML$ there appears a third maximum which corresponds to the resonant condition $v_{F1} + v_{F3}$. For $8ML$ and $9ML$ we observe the maxima which correspond to $2v_{F2}$.

In order to verify the validity of the resonant condition (25), in Fig. 8 we plot the positions of the first (black squares) and second (brown [dark gray] diamonds) maxima in the friction force as functions of film thickness and compare them with the positions of $2v_{F1}$ (red [gray] dots) and $v_{F1} + v_{F2}$ (blue [gray] triangles), also shown as functions of film thickness. We observe very good agreement which undoubtedly proves that the proposed mechanism is responsible for the friction maxima. Of course, these maxima are superimposed on the continua arising from the transitions from the initial states with velocities below v_{Fn}.

B. Quantum friction anomaly

Until now we were investigating the friction force between slabs using the jellium model, because up to the thickness of $8ML$ even a more realistic Chulkov model does not give
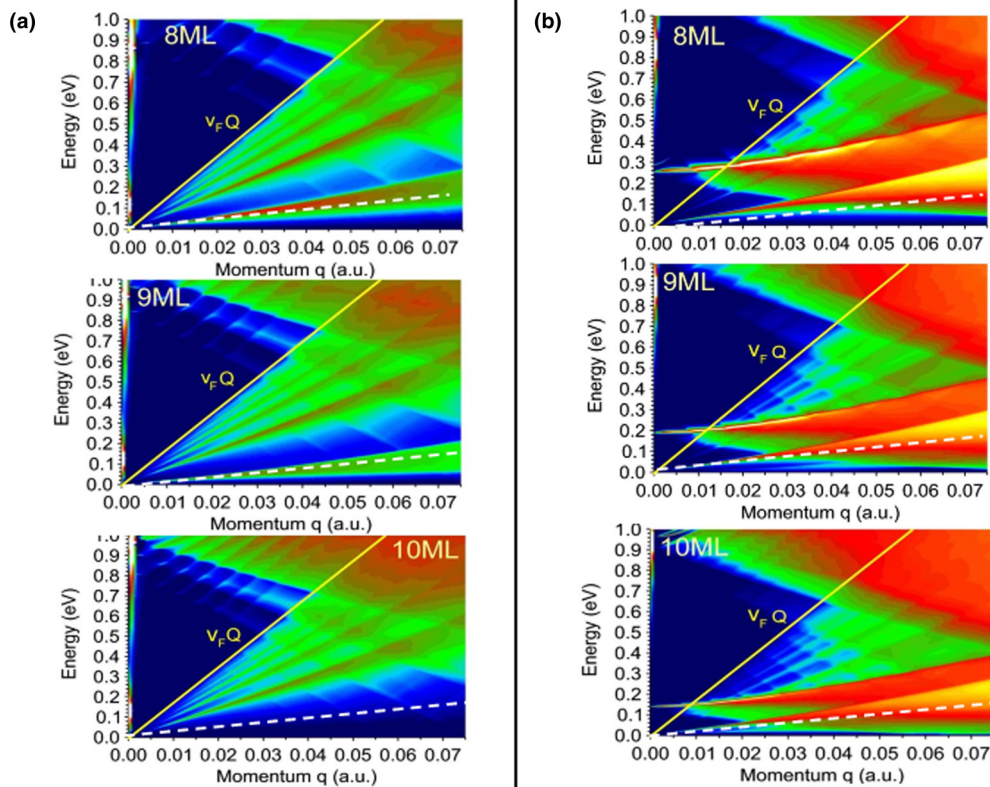
FIG. 6. (Color online) Intensities of the low-lying electronic excitations for different Ag(111) slab thicknesses (8, 9 and 10ML) in the (a) jellium and (b) Chulkov models. The color intensity is in arbitrary units and scales linearly as 0, black; 0.2, light blue; 0.4, light green; 0.6, red; 0.8, yellow; and 1.0, white.

qualitatively different results. However, friction forces in both models for thicknesses above 8ML show a very different behavior. Figure 9 shows the friction force between slabs in relative motion as a function of slab thickness. Relative velocity is $v = 0.1v_F$, and the separation between slabs is $d = 5$ nm. As can be noticed, for a 10ML-thick jellium slab the friction force (black squares) suddenly drops to zero, but at the same time the friction in the Chulkov model becomes strongly enhanced. The explanation for this anomaly can be
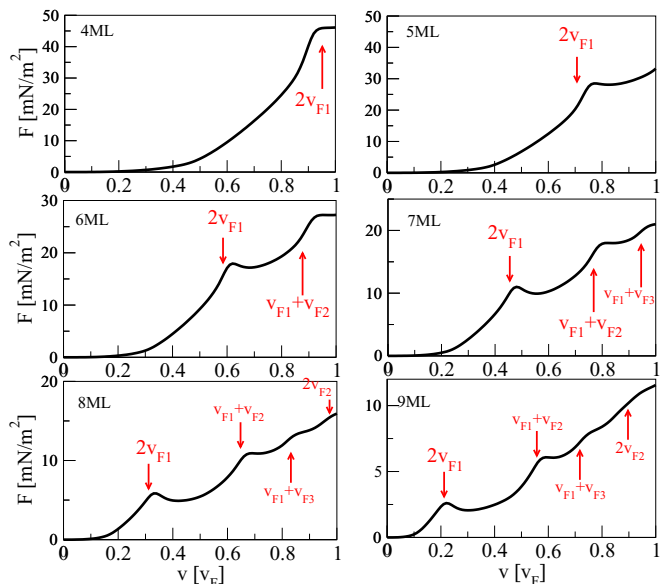

FIG. 7. (Color online) Friction force between jellium silver slabs in relative motion as function of relative velocity v with parameters given in the text. Red arrows show the position of corresponding Fermi velocities sums $v_{Fn} + v_{Fm}$.
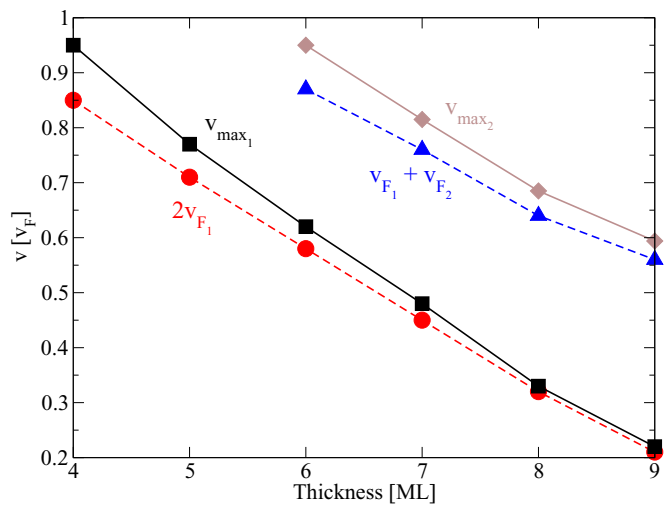

FIG. 8. (Color online) The positions of the first (black squares) and second (brown [dark gray] diamonds) maxima in the friction force as functions of metallic film thickness. Red (gray) dots show the positions of $2v_{F1}$, and blue (gray) triangles the position of $v_{F1} + v_{F2}$ as functions of film thickness.
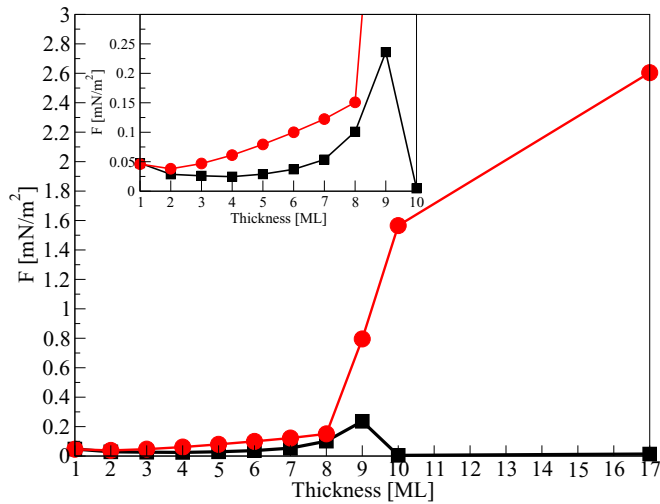
FIG. 9. (Color online) The friction force as function of silver film thickness in jellium model (black squares) and Chulkov model potential (red [gray] dots). Relative velocity is $v = 0.1 v_F$. Insert presents in more details the data in the $1-10 ML$ range.

found by analyzing the low-lying electronic excitations in both models, shown in Fig. 6.

Figure 6(a) shows electronic excitation intensities in $8ML$-, $9ML$-, and $10ML$-thick jellium slabs and Fig. 6(b) shows electronic excitation intensities in the same slabs described by the Chulkov model potential. White dashed lines denote the linear dispersion vQ where, to be consistent with the relative velocity in Fig. 9, we chose $v = 0.1 v_F$. Therefore all excitations in the area below the vQ line contribute to the friction force presented in Fig. 9. As the film thickness increases, the highest occupied band gradually becomes empty, as can be seen in Fig. 3. For $7ML$-, $8ML$-, and $9ML$-thick jellium slabs the highest occupied discrete band is still slightly below the Fermi level and supports low-lying intraband transitions with the dispersion approximately $v_{F1}Q$, also denoted by dashed lines in Fig. 6. In Fig. 6(a) we notice that such intraband excitations, for $8ML$ and $9ML$, lie below the vQ line and contribute to the friction force. However, for $10ML$ the highest occupied discrete band moves entirely above the Fermi level and becomes unoccupied. This causes the low-lying intraband transitions to disappear and the friction force drops to zero. However, for the Chulkov model potential we have a completely opposite effect. Namely, this potential supports two surface states, where one of them is partially occupied and another one is, for $7ML$ and $8ML$, unoccupied. However, for $9ML$, the upper surface state becomes partially occupied, as can be seen in Fig. 3, but enough to support the intraband electron-hole excitations with the dispersion below the vQ line. These excitations therefore now contribute strongly to the friction force.

We may comment on related work on graphene where electron-hole excitations can enhance quantum friction, though this does not correspond to quantum size effect. The phenomenon such as excitation of huge number of ultrasoft $\omega \approx 0$ intraband electron-hole pairs (the phenomenon which is responsible, e.g., for Drude conductivity) enables the quantum friction to become strongly enhanced and measurable. In

Ref. [32] it is shown how excitations of soft electron-hole pairs enhance friction between two graphene sheets. Graphene zero band gap and linear dispersion allow various mechanisms which can enhance quantum friction. For example, in pristine graphene interband $\pi \rightarrow \pi^*$ electron-hole transitions at the Dirac point lead to the finite density of excitations (JDOS) at $\omega = 0$, so the friction force becomes finite for small, measurable, relative velocities. In doped graphene the interband excitations shift to higher energies, i.e., at $\omega = 2E_F$ for $Q = 0$ (where E_F is a measure of doping relative to the Dirac point), and do not contribute to quantum friction. However, in doped graphene intraband $\pi \rightarrow \pi$ or $\pi^* \rightarrow \pi^*$ excitations enhance quantum friction in a manner similar to intraband transitions within the surface states bands, described previously. The upper edge of intraband ($\pi \rightarrow \pi$ or $\pi^* \rightarrow \pi^*$) excitations in doped graphene disperses as $\omega = v_F Q$, so the quantum friction will be strongly enhanced at $v \approx 2v_F$, when two intraband continua maximally overlap, as sketched in Fig. 4. Ideas on how to measure quantum friction are proposed in Ref. [31]. One idea consists of measuring the current-voltage characteristic of graphene deposited on the SiO_2 substrate. The charge carriers in graphene, beyond standard losses in graphene (phonons, impuryties, etc.), lose energy to excitations of optical phonons in the SiO_2 substrate which manifests as extra resistivity which can be easily measured. Another proposed option is to measure current drag between two graphene sheets, which induces voltage high enough to be easily detected experimentally.

C. Friction driven by acoustic surface plasmons

When the slab thickness increases further surface state energies become degenerate but always partially occupied, as can be seen in Fig. 3, which also shows the energies of even-odd surface states for $17ML$-thick silver slab. Therefore, the surface of a thick silver slab supports surface states which contain quasi-2D electron gas. At the same time, as can be seen, e.g., in the surface projected band structure in Fig. 2 of Ref. [30], there exists a continuum of bulk states which also contribute to the surface electronic density. Surface plasmas and projected bulk states hybridize at the surface and form a so-called acoustic surface plasmon (ASP) [39], which is characterized by a sound-like dispersion

$$\omega(Q) = v_{ASP} Q,$$

where the dispersion slope is defined as $v_{ASP} = \alpha v_{SS}$, with α being close to unity and v_{SS} being the surface state group velocity [40]. By analyzing the low-energy excitation spectra, e.g., spectra of $31ML$-thick silver slab shown in Fig. 5 of Ref. [30], we found that the ASP velocity is $v_{ASP} = 0.13 v_F$, which is very close to the surface state group velocity $v_{SS} = 0.11 v_F$, as predicted in Refs. [39,40]. In accordance with the previous analysis, the friction force between surfaces which support linearly dispersive modes has maxima at velocities given by the resonant condition (25). This suggests that the friction force between two silver surfaces which support surface states should be strongly enhanced, exactly at the velocity which is twice that of the acoustic surface plasmon phase velocity v_{ASP}. Although such a mode still was not detected on the Ag(111) surface it was
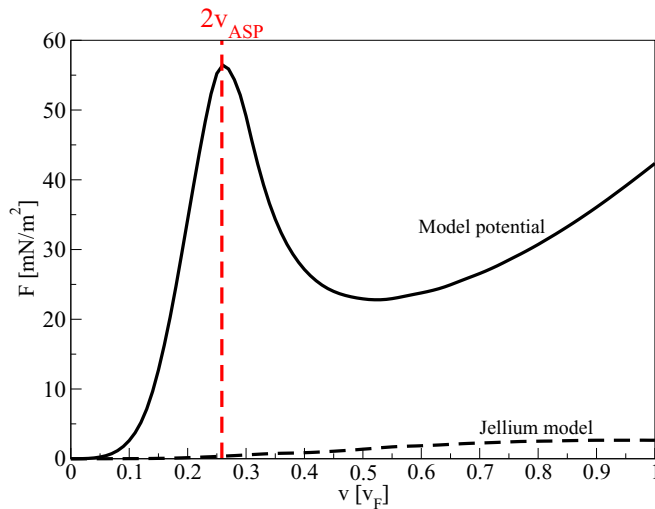
FIG. 10. (Color online) Friction force between two semi-infinite silver slabs in the jellium model (black dashed line) and in the Chulkov model potential (black solid line). Vertical red (gray) dashed line denotes the position of $v = 2v_{ASP}$.

observed in the loss experiments on a variety of metal surfaces supporting a similar partly occupied s-p surface state, like Be(0001) [41,42], Cu(111) [43–45], Au(111) [46,47], and Au(788) [48].

Figure 10 shows the friction force between two silver slabs separated by 5 nm as a function of their relative velocity. We see that if surfaces are described by the Chulkov potential (black solid line) the friction force shows a maximum which is placed exactly at $2v_{ASP}$, denoted by the dashed vertical line. However, friction force between jellium surfaces (black dashed line), which do not support surface states, is negligible.

IV. CONCLUSION

In this paper we demonstrate how a specific electronic structure influences the noncontact friction force between silver slabs. Depending on the slab thickness the friction force behavior can be divided into three regimes. Between $1ML$ and $8ML$ the quantum friction shows oscillations which are the consequence of quantum size effects. Main contribution to the friction comes from the soft intraband electron-hole excitations in the discrete bulk bands. This has enabled us to define resonant velocities (at which the friction force shows maxima) which are the sums of the Fermi velocities in discrete bands in the slabs 1 and 2. For $10ML$ the friction force shows an anomaly. Namely, in the jellium model it drops to zero while in the Chulkov model potential approach the friction becomes strongly enhanced. The reason is that in the jellium model the highest occupied band, exactly for $10ML$, becomes unoccupied while in the Chulkov model potential the surface state becomes partially filled, which opens an additional excitation channel. And finally, thick silver slabs support acoustic surface plasmons which represent a strong energy dissipation channel. This causes strong enhancement of the friction force for the relative velocity which is exactly equal to $2v_{ASP}$.

[1] R. Nunez, P. M. Echenique, and R. H. Ritchie, J. Phys. C **13**, 4229 (1980).

[2] T. L. Ferrell, P. M. Echenique, and R. H. Ritchie, Solid State Commun. **32**, 419 (1979).

[3] T. L. Ferrell and R. H. Ritchie, Phys. Rev. A **21**, 1305 (1980).

[4] J. F. Annett and P. M. Echenique, Phys. Rev. B **34**, 6853 (1986).

[5] V. M. Silkin, M. Alducin, J. I. Juaristi, E. V. Chulkov, and P. M. Echenique, J. Phys. Condens. Matter **20**, 304209 (2008).

[6] M. Alducin, V. M. Silkin, J. I. Juaristi, and E. V. Chulkov, Phys. Rev. A **67**, 032903 (2003).

[7] E. Buks and M. L. Roukes, Phys. Rev. B **63**, 033402 (2001).

[8] H. B. Chan, V. A. Aksyuk, R. N. Kleiman, D. J. Bishop, and F. Capasso, Science **291**, 1941 (2001).

[9] H. B. Chan, V. A. Aksyuk, R. N. Kleiman, D. J. Bishop, and F. Capasso, Phys. Rev. Lett. **87**, 211801 (2001).

[10] B. C. Stipe, H. J. Mamin, T. D. Stowe, T. W. Kenny, and D. Rugar, Phys. Rev. Lett. **87**, 096801 (2001).

[11] S. Kuehn, J. A. Marohn, and R. F. Loring, J. Phys. Chem. B **110**, 14525 (2006).

[12] S. Kuehn, R. F. Loring, and J. A. Marohn, Phys. Rev. Lett. **96**, 156103 (2006).

[13] G. Zolfagharkhani, A. Gaidarzhy, S.-B. Shim, R. L. Badzey, and P. Mohanty, Phys. Rev. B **72**, 224101 (2005).

[14] V. Teodorovich, Proc. R. Soc. London A **362**, 71 (1978).

[15] V. E. Mkrtchian, Phys. Lett. **207**, 299 (1995).

[16] J. B. Pendry, J. Phys. Condens. Matter **9**, 10301 (1997).

[17] B. N. J. Persson and Z. Zhang, Phys. Rev. B **57**, 7327 (1998).

[18] A. I. Volokitin and B. N. J. Persson, Phys. Rev. B **78**, 155437 (2008).

[19] J. B. Pendry, New J. Phys. **12**, 033028 (2010).

[20] J. B. Pendry, New J. Phys. **12**, 068002 (2010).

[21] A. I. Volokitin and B. N. J. Persson, Rev. Mod. Phys. **79**, 1291 (2007).

[22] A. I. Volokitin and B. N. J. Persson, Phys. Rev. B **83**, 241407 (2011).

[23] A. I. Volokitin and B. N. J. Persson, J. Phys. Condens. Matter **11**, 345 (1999).

[24] G. V. Dedkov and A. A. Kyasov, Surf. Sci. **604**, 562 (2010).

[25] J. S. Hye and I. Brevik, Eur. Phys. J. D **68**, 61 (2014).

[26] V. Despoja, P. M. Echenique, and M. Šunjić, Phys. Rev. B **83**, 205424 (2011).

[27] L. Marušić, V. Despoja, and M. Šunjić, Solid State Commun. **151**, 1363 (2011).

[28] L. Marušić, V. Despoja, and M. Šunjić, J. Phys. Condens. Matter **18**, 4253 (2006).

[29] E. V. Chulkov, V. M. Silkin, and P. M. Echenique, Surf. Sci. **437**, 330 (1999).

[30] V. M. Silkin, T. Nagao, V. Despoja, J. P. Echeverry, S. V. Eremeev, E. V. Chulkov, and P. M. Echenique, Phys. Rev. B **84**, 165416 (2011).

[31] A. I. Volokitin and B. N. J. Persson, Phys. Rev. Lett. **106**, 094502 (2011).

[32] A. I. Volokitin and B. N. J. Persson, Europhys. Lett. **103**, 24002 (2013).

[33] V. Despoja, D. Novko, K. Dekanić, M. Šunjić, and L. Marušić, Phys. Rev. B **87**, 075447 (2013).

[34] V. Despoja, M. Šunjić, and L. Marušić, Phys. Rev. B **75**, 045422 (2007).

[35] V. Despoja, M. Šunjić, and L. Marušić, Phys. Rev. B **83**, 165421 (2011).

[36] Z. Penzar and M. Šunjić, Phys. Scr. **30**, 431 (1984).

[37] L. Marušić and M. Šunjić, Phys. Scr. **63**, 336 (2001).

[38] N. W. Ashcroft and N. D. Mermin, *Solid State Physics* (Harcourt College Publishers, Orlando, FL, 1976).

[39] V. M. Silkin, J. M. Pitarke, E. V. Chulkov, and P. M. Echenique, Phys. Rev. B **72**, 115435 (2005).

[40] J. M. Pitarke, V. U. Nazarov, V. M. Silkin, E. V. Chulkov, E. Zaremba, and P. M. Echenique, Phys. Rev. B **70**, 205403 (2004).

[41] B. Diaconescu, K. Pohl, L. Vattuone, L. Savio, P. Hofmann, V. M. Silkin, J. M. Pitarke, E. V. Chulkov, P. M. Echenique, D. Farías, and M. Rocca, Nature (London) **448**, 57 (2007).

[42] M. Jahn, M. Müller, M. Endlich, N. Néel, J. Kröger, V. Chis, and B. Hellsing, Phys. Rev. B **86**, 085453 (2012).

[43] K. Pohl, B. Diaconescu, G. Vercelli, L. Vattuine, V. M. Silkin, E. V. Chulkov, P. M. Echenique, and M. Rocca, Europhys. Lett. **90**, 57006 (2010).

[44] L. Vattuone, G. Vercelli, M. Smerieri, L. Savio, and M. Rocca, Plasmonics **7**, 323 (2012).

[45] J. Pischel, E. Welsch, O. Skibbe, and A. Pucci, J. Phys. Chem. C **117**, 26964 (2013).

[46] S. J. Park and R. E. Palmer, Phys. Rev. Lett. **105**, 016801 (2010).

[47] L. Vattuone, M. Smerieri, T. Langer, C. Tegenkamp, H. Pfnür, V. M. Silkin, E. V. Chulkov, P. M. Echenique, and M. Rocca, Phys. Rev. Lett. **110**, 127405 (2013).

[48] M. Smerieri, L. Vattuone, L. Savio, T. Langer, C. Tegenkamp, H. Pfnür, V. M. Silkin, and M. Rocca, Phys. Rev. Lett. **113**, 186804 (2014).